14th World Congress on Computational Mechanics (WCCM)
ECCOMAS Congress 2020)
Virtual Congress: 11-–15 January 2021
F. Chinesta, R. Abgrall, O. Allix and M. Kaliske (Eds)

NUMERICAL ANALYSIS OF OSCILLATORY FLOWS IN THE HUMAN BRAIN BY A LATTICE-BOLTZMANN METHOD

SEONG-RYONG KOH[1], JONG-HYUN KIM[2] AND ANDREAS LINTERMANN[3]

[1] Jülich Supercomputing Centre
Forschungszentrum Jülich, Wilhelm-Johnen-Straße, 52425 Jülich, Germany
Email: s.koh@fz-juelich.de
https://www.fz-juelich.de/ias/jsc

[2] Korea University Medicine
Korea University Guro Hospital, 148 Gurodong-ro Guro-gu, 08308 Seoul, Korea
http://guro.kumc.or.kr/language/ENG/main/index.do

[3] Jülich Supercomputing Centre
Forschungszentrum Jülich, Wilhelm-Johnen-Straße, 52425 Jülich, Germany
https://www.fz-juelich.de/ias/jsc

Key words: cerebrospinal fluid, brain ventricular system, lattice-Boltzmann method

Abstract. The cerebrospinal fluid flow in a brain ventricular system is analyzed by the numerical approach employing a lattice-Boltzmann (LB) method. The cerebrospinal fluid, which surrounds the human brain and spinal cord, fills the cerebral ventricles as well as the cranial and subarachnoid spaces. Diseases in a central nerve system disrupt the flow circulation which influences on a number of vital functions. A computational fluid dynamics technique is used to determine the member geometry impact on the flow motion. The numerical analysis focuses on building a simulation-based basis for testing/optimizing therapeutical methods and understanding the pathophysiology. Magnetic resonance (MR) imaging is exploited to obtain realistic geometries in a brain ventricular system. The computational domain is discretized by a hierarchical Cartesian octree mesh. The numerical procedure based on an LB method overcomes the difficulties raised by typical finite-difference and finite-volume methods on high-performance computing (HPC) systems. An oscillating flow boundary condition is defined to resolve the kinetic behavior of cerebrospinal fluid in a cardiac cycle. The three-dimensional structures captured in the cerebral ventricles show a qualitative agreement with an observation based on an MR velocity mapping. The simulation on a HPC system is able to provide further insights into the transport from brain to spinal cord.

1 INTRODUCTION

The cerebrospinal fluid (CSF) fills the cerebral ventricles as well as the cranial and subarachnoid spaces (SAS). Circulating in the brain and the spinal cord, the CSF transports nutrients and neuroendocrine substances and removes toxic chemicals to preserve the healthy environment inside a brain[1]. The flow pulsates through two lateral ventricles, which are connected with the third ventricle. A thin channel, i.e., the aqueduct of Sylvius, communicates with the third and the fourth ventricle. The CSF is transferred

from the fourth ventricle to the cranial and spinal SAS. Diseases in the central nerve system immediately impacts on a number of vital functions, e.g., disruption in CSF circulation. In clinic the intracranial pressure (ICP) is monitored in neurosurgical practice since the ICP variation in time reflects pathological symptoms associated with CSF pressure changes. The values are used in diagnosis and the treatment of diseases inside the cerebral flow network[2,3]. The baseline pressure level is affected by periodic components coming from the cardio-respiratory activity. Fluctuation of mean arterial pressure with heart rate causes small amplitude rapid pulsation, and respiration causes larger amplitude fluctuations of lower frequency. ICP is completely described only by information about both the baseline level and the pulsating components[2]. Several prominent disease states deduce from disorders of the CSF dynamics. This includes, e.g., an increased intracranial pressure by hydrocephalus[4] or decreases in the flow and pulsatility by Chiari malformations[5]. However, the clinical decision making is difficult when the symptom occurs with no disease characteristics as observed in normal pressure hydrocephalus. Unfortunately, the specific etiologies and the biomechanical interactions between the components of the central nerve system (CNS) are hardly understood under abnormal fluid conditions.

The basic physiologic concept about the CSF and ICP started already in the early 19th century. So called the Monro-Kellie doctrine[6,7] is formalized as the fundamental concept reads

$$V_{\mathrm{CSF}} + V_{\mathrm{Blood}} + V_{\mathrm{Brain}} + V_{\mathrm{Other}} = V_{\mathrm{Intracranial\ space}} = \text{constant}, \tag{1}$$

where V_{CSF} is volume of CSF, V_{Blood} is volume of blood, V_{Brain} is volume of brain, and V_{Other} is volume of any abnormal component, such as a tumor. This equation provides a general framework for understanding pathologic causes of elevated ICP and also its treatments since 1950s[8]. For adults, the volume of cerebrospinal fluid is 165 mL, which varies from 62 mL to 267 mL, in cranium. About 99% of CSF is water. The water solution contains approximately 0.3% plasma proteins, and is normally free of red blood cells. The major portion of fluid is produced by the choroid plexus, i.e., a network of blood vessels within sections of the brain ventricles. The choroid plexus is present throughout the ventricular system except for the cerebral aqueduct and the frontal and occipital horns of the lateral ventricles[9,10]. The CSF production starts from a filtered form of plasma with movement guided by a difference in pressure between the blood in the capillaries and the interstitial fluid. Afterwards, this fluid needs to pass through the epithelium cells lining the choroid plexus into the ventricles. An active process requires the transport of sodium, potassium and chloride that draws water into CSF by creating osmotic pressure. And this transcellular fluid is constantly absorbed again such that only a certain amount of fluids is present at any one time. An equivalent circuit model of the flow network described the formation, storage, and the absorption at a given intracranial pressure[11]. According to this model the intracranial pressure value can be determined by the CSF formation current, a single resistance element, and the pressure in the dural sinuses. As introduced in the previous slides, the ICP signal has a baseline value and the amplitude of the fluctuations remain almost constant at a normal condition.

The Monro-Kellie hypothesis implies that a brain disease due to abnormal components makes reciprocal changes in the volumes of brain, blood, and cerebrospinal fluids to preserve the ICP. The main motivation of the current study is to determine the CSF motion based on the fundamental hypothesis. Furthermore, in surgical practice the external or the internal drainage is chosen as treatment to control the high ICP values[12]. Although doctors also use other methods with medication, the treatment of hypertension is typically mechanical for the fluid volume. The detailed fluid dynamic analysis is able to provide a better understanding of the CSF flow behavior in the complex brain ventricular system. Computational fluid

dynamics can be used to quantify the functional interactions of the members of the ventricular system.

In the aforementioned clinical applications[8,11,12] the fluid circulation models consider the pressure dynamics and the dynamics of CSF and cerebral blood flow. The quantitative assessment provides robust evidences in judging a patient care when the clinical parameters are subtle and ambiguous[1,13]. The fluid dynamics model exploited in the numerical analyses is based on the fundamental conservation law of mass, momentum, and chemical reactions[14–16]. The approaches using computational fluid dynamics (CFD) can simulate realistic CSF flows to predict the patient-specific scenarios. The present study aims to establish a basis to test and optimize a clinical therapy via the anatomically accurate simulation based on a robust numerical procedure.

The three-dimensional images obtained by magnetic resonance imaging (MRI) provide the structures of ventricles and the SAS. For a normal healthy human the CSF speed ranges in several centimeters per second. The typical Reynolds number is in the order of $O(10^2)$. However, the physiological mechanisms of the CSF circulation develop vortical flow structures which exhibit a turbulent-like motion induced by the difference in systolic and diastolic velocities and the interactions of micro-structures with fluids[15,16]. To resolve the micro-structures, like nerve roots and trabeculae, a short spinal segment already demands a significant increase of the computational cost[15]. These fluid dynamic and the computational difficulties obstruct the development of a therapeutic basis in medical diagnosis.

In the present numerical study, the complex anatomical geometries as well as the CSF pulsatility are tackled with the high-resolution computations using the high-performance computing (HPC) technique. The numerical solutions of transitional phases will be validated on the quantitative assessment based on literature[13,17]. The impact of pulsatility on the flow dynamics will be investigated by a generic flow configuration such that the fundamental findings can be applied to other engineering problems. The outcomes of this study have the potential to be expanded to various areas within fluid mechanics and the numerical models of CNS. Together with the clinical researches the high-resolution CFD analysis will enable a better understanding of the pathophysiological basis of a number of diseases causing dysfunction of CSF circulation.

The structure of the paper is as follows. In section 2 the numerical method and the parallel mesh generation are described. Then, the geometries obtained by MR image manipulation in section 3 and the flow configuration in section 4 are defined. Subsequently, the numerical result of the high resolution numerical method is discussed in section 5. Finally, the major findings are summarized in section 6.

2 NUMERICAL METHODS

2.1 Lattice-Boltzmann method

The simulation of CSF flows is performed with a lattice-Boltzmann (LB) method in the quasi-incompressible flow regimes. By solving the microscopic distribution of the fluid particles the LB method can determine flow fields in a simpler manner than the typical finite-difference and finite-volume approaches. The LB algorithm is completely local operation and its locality ensures a massive parallelism on the high-performance computing (HPC) system. The LB method is validated in generic flow configurations[18,19] and has been applied to bio-fluid mechanical problems[20,21].

In the single-relaxation-time (SRT) LB method, the Boltzmann equation with the Bhatnagar-Gross-Krook (BGK) approximation of the right-hand-side collision term[22] is solved for the particle probability

distribution functions f_i (PPDFs) in a discretized form

$$f_i(\mathbf{x}+\xi_i\Delta t, t+\Delta t) = f_i(\mathbf{x},t) - \omega_{SRT}(f_i(\mathbf{x},t) - f_i^{eq}(\mathbf{x},t)), \tag{2}$$

where $\mathbf{x} = (x_1, x_2, x_3)^T$ and $\xi_i = (\xi_1, \xi_2, \xi_3)^T$ are the position and molecular velocity vectors, t is the time and Δt its increment. The discrete Maxwellian distribution function f_i^{eq} is determined by

$$f_i^{eq}(\mathbf{x},t) = \rho t_p \left[1 + \frac{u_a\xi_{ia}}{c_s^2} + \frac{u_a u_b}{2c_s^2} \cdot \left(\frac{\xi_{ia}\xi_{ib}}{c_s^2} - \delta_{ab}\right)\right]. \tag{3}$$

This discretized formulation consists of a fluid density ρ, direction-dependent weighting factors t_p, an isothermal speed of sound $c_s = 1/\sqrt{3}$, velocity components u_a and u_b of the fluid velocity vector $\mathbf{u}$, and the Kronecker delta δ_{ab} with $a, b \in \{1,2,3\}$. The quantity ω_{SRT} is the relaxation factor

$$\omega_{SRT} = \frac{c_s^2}{\nu + \Delta t c_s^2/2} \tag{4}$$

with viscosity ν. The parameter i in Eqs. (2) and (3) is chosen by the D3Q27 discretization scheme[23] with 27 direction in a three dimensional flow field. The macroscopic variables can be obtained from the moments of the PPDFs[24]

$$\rho = \sum_i f_i(\mathbf{x},t) \tag{5}$$

$$\rho u_a = \sum_i \xi_{ia} f_i \mathbf{x},t) \tag{6}$$

$$\rho(e + u_a^2) = \frac{1}{2}\sum_i \xi_{ia}^2 f_i(\mathbf{x},t) \tag{7}$$

$$\rho u_a u_b + p\delta_{ab} - \sigma_{ab} = \sum_i \xi_{ia}\xi_{ib} f_i(\mathbf{x},t), \tag{8}$$

where the pressure can be obtained from

$$p = \rho c_s^2. \tag{9}$$

The computations are performed in non-dimensional space. The non-dimensional molecular velocity components $\xi_{ia} = \tilde{\xi}_{ia}/\tilde{\xi}_0$ are obtained from the dimensional molecular velocity components $\tilde{\xi}_{ia}$ and the reference molecular velocity $\tilde{\xi}_0$. The non-dimensionalization of the density $\rho = \tilde{\rho}/\tilde{\rho}_0$ uses the reference density $\tilde{\rho}_0$. The reference fluid velocity U_0 in the simulation is obtained from the Mach number $\mathrm{Ma} = U_0/c_s$ used in the LB simulation. The viscosity in the simulation is obtained by means of the Reynolds similarity, i.e, the Reynolds number $Re = U_0\tilde{L}/\tilde{\nu}$ with reference velocity magnitude U_0, reference length $\tilde{L}$ and fluid viscosity $\tilde{\nu}$ are used to obtain the non-dimensional viscosity via

$$\nu = \tilde{\nu} \cdot \mathrm{Ma} \cdot \frac{c_s}{U_0} \cdot \frac{L}{\tilde{L}}, \tag{10}$$

where $L = \tilde{L}/\Delta\tilde{x}$. The relation of the pressure uses Eq. (9) for conversion. All results presented in Sec. 5 are in their non-dimensional form.

2.2 Grid generation

A hierarchical Cartesian computational mesh is generated using the massively parallel method presented in[25]. That is, each message passing interface (MPI) process initially generates a cube, in the following referred to as cell, around the geometry with an edge length of the maximum extent of the geometry in the three Cartesian coordinate axes. Subsequently, this cube is subdivided into eight child cells constituting an octree with parent-child relationships between the initial cell on level l_0 and its descendants on level l_1. Cells outside the geometry are identified and removed from the tree. The subdivision process then recursively continues the refinement up to a user-defined level l_m. On l_m, all levels l_j ($j < m$) are removed and a Hilbert curve is placed in the remaining cells. The computational mesh is then equally distributed among the MPI processes by cutting the Hilbert curve with respect to the Hilbert identifier. Thereby, each process keeps only those cells that have been assigned to it.

In a parallel algorithm each MPI process subsequently starts to continue the refinement up to a user-defined level l_n. Finally, neighborhood information across MPI ranks is globally restored and a cell ordering is introduced following the Hilbert curve on level l_m and a z-ordering, i.e., a depth-first ordering, for all levels l_k ($m < k \leq n$). Process imbalances are treated by a load-balancing technique. For further details, the reader is referred to[25]. The geometry of brain ventricles is obtained by manipulation of MRI scans. The procedure of medical images is described in the following section 3.

3 GEOMETRY

The flow simulation of a brain ventricular system is performed to establish a basis for supporting the diagnostic procedure. The understanding of pathology and the biofluid dynamics is able to improve the therapeutic methods. In the flow simulation the geometry of ventricles and subarachnoid space is obtained by segmentation of cerebrospinal fluid regions. The fluid is identified by the T1-weighted MRI scans shown in Fig. 1. The MRI scan using the SIMENS Magnetom-Skyra examined the main cranial nerves region of a normal adult. The personal data is anonymized. The three-dimensional MRI scan

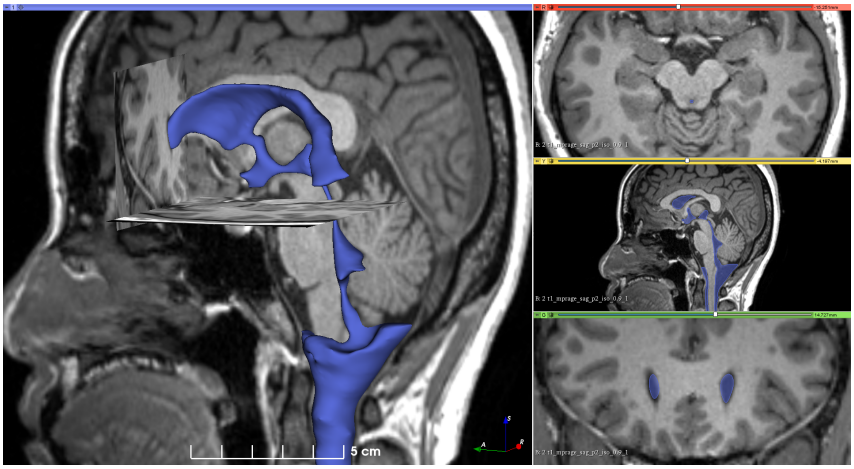

Figure 1: Segmentation of a brain ventricular system visualized by the T1-weighted MRI scans; in the left a main window shows the blue three-dimensional structure used in the flow simulation, and in the right three sub-windows show the segmentation colored by blue.

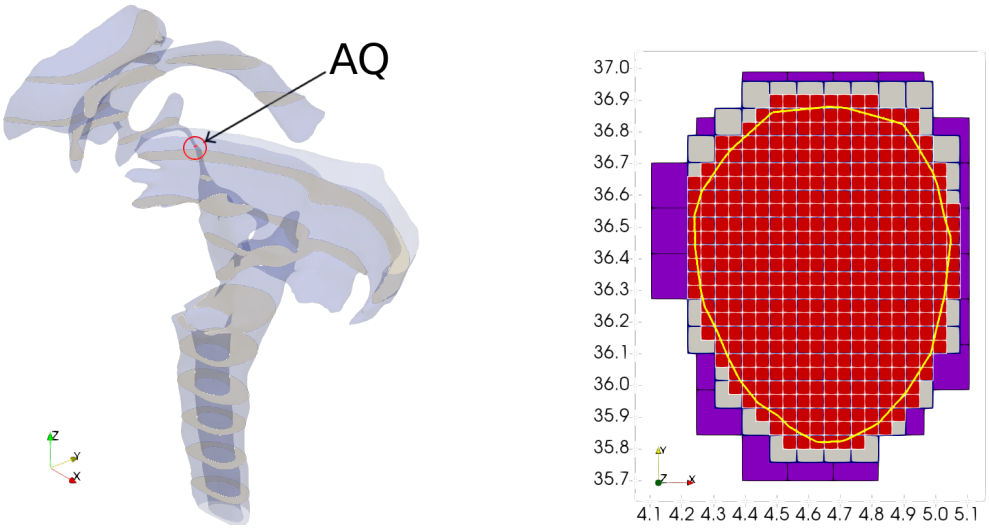

(a) (b)

Figure 2: Geometry of brain ventricles obtained by segmentation of CSF region, (a) brain ventricles and subarachnoid space, (b) an enlarged view of meshes in the cross-section (AQ) at the aqueduct of Sylvius where the unit of length is the millimeter (mm).

generates 192 slices with a thickness 0.9 mm in the sagittal direction. Each slice consists of 256×256 pixels with a pixel spacing of 0.898 mm.

The computational domain is discretized by a hierarchical Cartesian octree mesh. The computational mesh is generated by the procedure described in section 2.2. The segmentation was manipulate by the free-and-open source software 3D Slicer[26]. The STL (Standard Triangle Language) format geometry is presented in Fig. 2(a). The numerical mesh in a cross-sectional area AQ is illustrated in Fig. 2(b). At the refinement level 11 (red meshes) the computational domain consists of $193,289,733$ numerical cells. The characteristic length of the LB method is 390.33 cell units.

4 FLOW CONFIGURATION

The MRI manipulation generates a realistic geometry of a brain ventricular system. The commonly faced issues in studying biofluid dynamics are boundary conditions of a finite computational domain. The variation of intracranial pressure is an essential parameter for the flow configuration. In the following section the configuration of a ventricular system is detailed with model geometries and an oscillating flow boundary condition.

4.1 Flow oscillation and non-dimensional frequency

The Monro-Kellie doctrine implies that a brain disease due to abnormal components makes reciprocal changes in the volumes of brain, blood, and cerebrospinal fluids to preserve the intracranial pressure. The flow simulation is configured by the pressure variation as an only factor that impacts on the CSF dynamics. The pressure values at the inflow and the outflow boundaries are determined by the steady flow condition with the constant flow properties. Since the flow motion in brain ventricles is oscillating

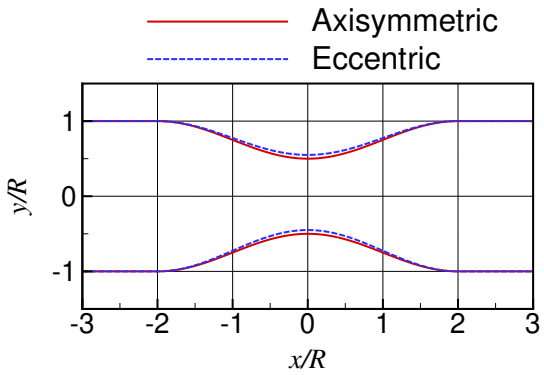

Figure 3: Profiles of an axisymmetric and an eccentric pipe near the stenosis at the x-coordinate $x = 0$, the profiles are scaled by a radius R ($= D/2$).

with respect to the cardiac cycles. The oscillation frequency is defined by Womersley number Wo

$$\mathrm{Wo} = L\sqrt{\frac{\omega\rho}{\mu}}, \tag{11}$$

where $\omega = 2\pi f$ is angular frequency, μ is the dynamic viscosity, and ρ is the density of fluid. In the present study the pipe diameter D is chosen as a reference length L. Concerning a reference velocity U a non-dimensional frequency St can be calculated using Eq. (11) as following

$$\mathrm{St} = \frac{fD}{U} = \frac{\mathrm{Wo}^2}{2\pi\,\mathrm{Re}_D}, \tag{12}$$

where $\mathrm{Re}_D = \rho UD/\mu$ is the Reynolds number based on on a diameter D.

4.2 Generic model and ventricular system

The Steady and oscillating flows through both axis-symmetric and eccentric stenotic flow models were analyzed with both stenosis geometries corresponding to 25% area at the location of the restriction compared to the inflow area. The baseline stenosis geometry is similar to that used in the stenotic flow experiments[27]. The profiles of the axis-symmetric and eccentric stenosis models are defined by following equations. A cosine function dependent on the axial coordinate x is used to generate the geometry. The cross-section coordinates y and z are determined by using $S(s)$ specifying the shape of the stenosis by

$$S(x) = R\Big[1 - s_0\Big(1 + \cos(2\pi x/L)\Big)\Big], \quad E(x) = 0.1s_0\Big[1 + \cos(2\pi x/L)\Big], \tag{13}$$

where R is the radius of the non-stenotic pipe, $s_0 = 0.25$ realizes the 75% area reduction, and $L = 4R$ is the length of the stenosis. By introducing the eccentricity $E(x)$, the y and z coordinates are defined by

$$y = S(x)\cos\theta + E(x), \quad z = S(x)\sin\theta, \tag{14}$$

at the azimuthal angle θ on the yz-plane. The axis-symmetric and the eccentric pipe are defined by Eqs. (13) & (14) with a 5% eccentricity at $x/R = 0$. In Fig. 3 the cross-section profiles of a axisymmetric and a eccentric pipe is illustrated near the stenotic region at $x = 0$.

For the ventricular system the CSF oscillation in brain ventricles possesses pressure variation in a cardiac cycle. The temporal variation of pressure is defined at the lateral ventricles. The Reynolds number Re_D is defined by a hydraulic diameter ca. 16.7 mm near the exit of the 4th ventricle. The peak Reynolds number is ca. 628 at the Womersley number $\mathrm{Wo} = 15$[28]

5 RESULTS

The numerical analysis focuses on the CSF motion which is determined by an oscillating flow boundary condition with the geometry of brain ventricular system connected to the cranial and the spinal SAS. At the beginning two isolated stenotic pipes are considered with the median aperture which mimics drainage from the ventricles to the subarachnoid space.

5.1 Isolated stenotic pipe flow

The numerical analysis using a generic configuration is performed to detail the instantaneous and statistical flow features which occur downstream of a stenosis under the oscillating flow condition. The non-dimensional parameters defined in Section 4 are chosen to provide a fundamental basis for understanding the flow dynamics generated by even more complex occlusions within the ventricle system and SAS in the human CNS. The peak Reynolds number is 600 based on the pipe diameter. The flow oscillation is defined by a sinusoidal function at the Womersley number $\mathrm{Wo} = 15$ scaled by the pipe diameter. In Fig 4 the contours of density and velocity distributions are presented at the peak pressure on the right boundary surface. The axisymmetric configuration develops a symmetric form of shear layers. The flow mixing in Fig. 4(b) is pronounced by an asymmetric geometry at the stenosis.

Figure 5 shows the impact of the shear-layer mixing on the intensity of velocity fluctuations. In the eccentric pipe the turbulent shear stress increases at the downstream such that the peak location is further shifted to the wall compared to the result of axisymmetric stenotic pipe.

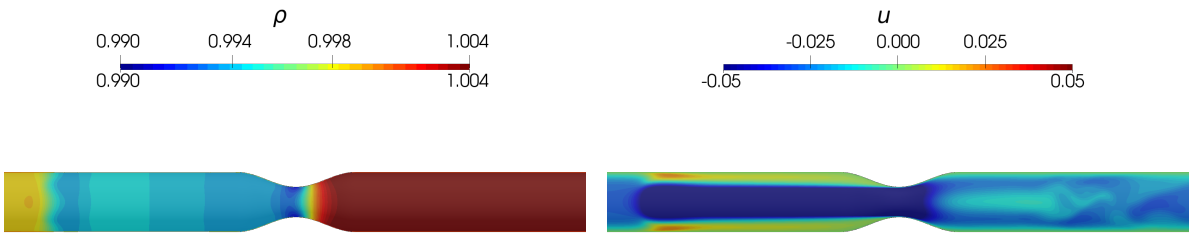

(a) Axisymmetric pipe

(b) Eccentric pipe

Figure 4: Contours of density and velocity component determined by an axisymmetric and an eccentric stenotic pipe, (a) axisymmetric pipe, (b) eccentric pipe.

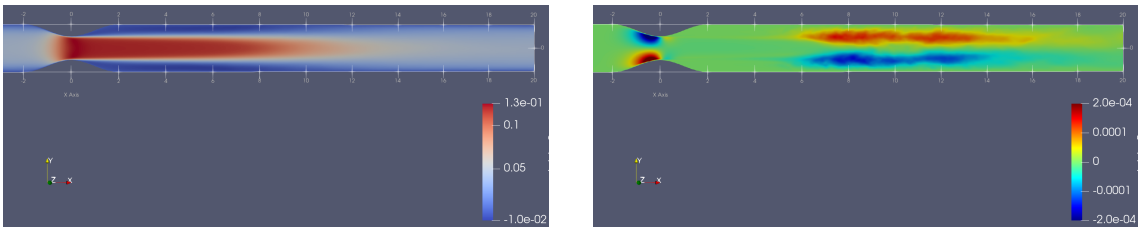

(a) Axisymmetric pipe (left: $\overline{u}$, right: $\overline{u'v'}$)

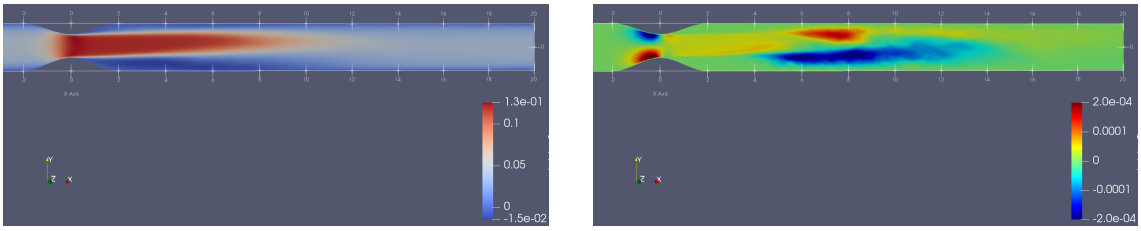

(b) Eccentric pipe (left: $\overline{u}$, right: $\overline{u'v'}$)

Figure 5: Contours of time-averaged u-velocity and a component of turbulent shear stresses $\overline{u'v'}$, (a) axisymmetric pipe, (b) eccentric pipe.

5.2 CSF motion inside ventricles

In the CSF flow simulation the hydraulic diameter 16.7 mm is obtained at a cross-section between the 4th ventricle and the central canal to the spinal cord. The Reynolds and the Womersley number scaled by the diameter at the aqueduct of Sylvius is equivalent to the flow condition in the experimental studies[17,28]. The variation of intracranial pressure is correlated with the pathology of cerebrospinal fluid[12]. The pressure oscillation in the lateral ventricles defines the systolic and diastolic phase in this numerical analysis. In section 5.1 the small eccentricity increases the shear stresses in the pipe flow. That is, the well-defined geometries of a brain ventricular system are required to predict the CSF flow field in a healthy and a dysfunctional CNS. The simulation shows that the flow instabilities are pronounced

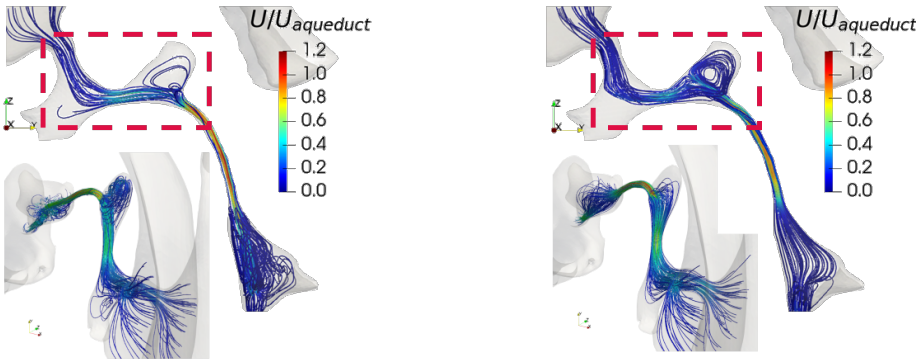

(a) Systole (b) Diastole

Figure 6: Streamlines in the 3rd ventricle, the color indicates a velocity magnitude normalized by the mean velocity of the aqueduct of Sylvius, (a) systole phase, (b) diastole phase.

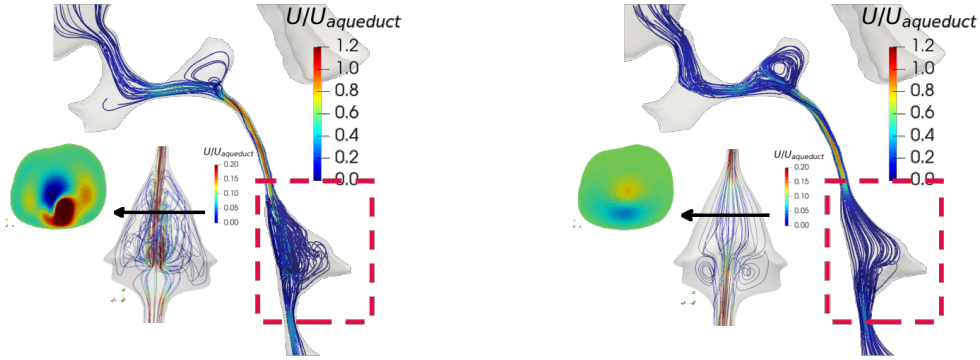

(a) Systole (b) Diastole

Figure 7: Streamlines in the 4th ventricle and contours of the v-velocity component at a cross section, the color indicates a velocity magnitude normalized by the mean velocity of the aqueduct of Sylvius, (a) systole phase, (b) diastole phase.

by geometry effects. The flow oscillation in ventricle channels trigger the turbulence transition in the ventricles. Figure 6 shows the streamlines inside the brain ventricles at a systolic and a diastolic phase. The enlarged images are chosen to focus on the flow motion between the lateral and the 3rd ventricles.

Figure 7 shows the streamlines inside the 4th ventricle at a systolic and a diastolic phase. The cross-section is located at an axial position near the aqueduct of Sylvius. The contours in this cross-section are the v-velocity component, i.e., the positive values are in the posterior direction. In Fig. 7(a) at a systolic phase two main circulations appear inside the 4th ventricle. The secondary flow on the cross-section is induced by the flow passage diverging from the cerebral aqueduct. This secondary flow does not occur in the diastolic phase in Fig. 7(b). The current flow simulation captures the circulation at the systolic and the diastolic phase, i.e., the streamlines determined in the 3rd and the 4th ventricle (Figs. 6&7), which was observed in the measurements using magnetic resonance (MR) velocity mapping[17].

6 CONCLUSIONS

- The simulation of a flow oscillation in brain ventricles was performed by using the lattice Boltzmann (LB) method in the quasi-incompressible regimes for the cerebrospinal fluid motion. The LB method is a powerful numerical solver to complex flow geometry and easily extended to massive parallelization on HPC platforms.
- The geometry of a brain ventricular system was obtained by segmentation of the cerebrospinal fluid which is visualized by the T1-weighted MRI scans. The surface extraction required manual operations to detail the members of central verve system. The main issue was the resolution of the medical images which restricted by the current hardware constraints and practical difficulties. A new approach such as the super resolution via deep learning is necessary to define characteristics and to preserve the contents details in future.
- An oscillating flow boundary condition is defined by the pressure variation at a Womersley number. The CSF motion is captured at the systole and the diastole phase in a cardiac cycle such that the streamline shows a good agreement with the observation based on an MR velocity mapping.

ACKNOWLEDGEMENTS

The authors gratefully acknowledge the computing time granted through the Jülich Aachen Research Alliance (JARA) on the supercomputer JURECA[29] at Forschungszentrum Jülich.

REFERENCES

[1] Linninger, A., Tangen, K., Hsu, C.-Y., Frim, D. Cerebrospinal fluid mechanics and its coupling to cerebrovascular dynamics. *Ann. Rev. Fluid Mech.* (2016) **48**:219–257.

[2] Dunbar, H. S., Guthrie, T. C., Karpell, B. A. A study of the cerebrospinal fluid pulse wave. *Arch. Neurol.* (1966) **14**(6):624–630.

[3] Hamer, J., Alberti, E., Hoyer, S. et al. Influence of systemic and cerebral vascular factors on the cerebrospinal fluid pulse waves. *J. Neurosurg.* (1977) **46**(1):36–45.

[4] Balédent, O., Gondry-Jouet, C., Meyer, M.-E., De Marco, G., Le Gars, D., et al. Relationship between cerebrospinal fluid and blood dynamics in healthy volunteers and patients with communicating hydrocephalus. *Invest. Radiol.* (2004) **39**(1):45–55.

[5] Armonda, R. A., Citrin, C. M., Foley, K. T., Ellenbogen, R. G. Quantitative cine-mode magnetic resonance imaging of Chiari I malformations: an analysis of cerebrospinal fluid dynamics. *Neurosurgery* (1994) **35**(2):214–224.

[6] Monro, A. *Observations on the Structure and Functions of the Nervous System*. Edinburgh: William Creech & Johnson (1783).

[7] Kellie, G. An account of the appearances observed in the dissection of two of three individuals presumed to have perished in the storm of the 3rd, and whose bodies were discovered in the vicinity of Leith on the morning of the 4th, November 1821; with some reflections on the pathology of the brain. *Trans. Med. Chir. Soc. Edinburgh* (1824) **1**:84–169.

[8] Guillaume, J. and Janny, P. Continuous intracranial manometry; importance of the method and first results. *Rev. Neurol.* (1951) **84**:131–142.

[9] Hunter, G. and Smith, H. V. Calcium and magnesium in human cerebrospinal fluid. *Nature* (1960) **186**:161–162.

[10] Hendry, E. B. The osmotic pressure and chemical composition of human body fluids. *Clin. Chem.* (1962) **8**:246–265.

[11] Marmarou, A., Barzo, P., Fatouros, P., et al. Traumatic brain swelling in head injured patients: brain edema or vascular engorgement? *Acta. Neurochir. Suppl. Wien* (1997) **70**:68-70.

[12] Beaumont, A. *Physiology of the cerebrospinal fluid and intracranial pressure*. Youmans Neurological Surgery, 6th Edition, (2011).

[13] Czosnyka, M., Czosnyka, Z., Balédent, O., Weerakkody, R., Kasprowicz, M., Smielewski, P., Pickard, J. *Dynamics of cerebrospinal fluid: from theoretical models to clinical applications*. Biomechanical Engineering of the Brain, Editor: Miller, K., Springer (2011).

[14] Gupta, S., Soellinger, M., Grzybowski, D. M., Boesiger, P., Biddiscombe, J., Poulikakos, D., Kurtcuoglu, V. Cerebrospinal fluid dynamics in the human cranial subarachnoid space: an

overlooked mediator of cerebral disease. I. computational model. *J. Roy. Soc. Interface* (2010) **7**(49):1195–1204.

[15] Tangen, K., Hsu, Y., Zhu, D., Linninger, A. CNS wide simulation of flow resistance and drug transport due to spinal microanatomy. *J. Biomech.* (2015) **48**(10):2144–2154.

[16] Khani, M., Sass, L. R., Xing, T., Sharp, M. K., Balédent, O., Martin, B. A. Anthropomorphic model of intrathecal cerebrospinal fluid dynamics within the spinal subarachnoid space: spinal cord nerve roots increase steady-streaming. *J. Biomech. Eng.* (2018) **140**(8):081012-1.

[17] Stadlbauer, A., Salomonowitz, E., van der Riet, W., Buchfelder, M., Ganslandt, O. Insight into the patterns of cerebrospinal fluid flow in the human ventricular system using MR velocity mapping. *NueroImage* (2010) **51**(1):42–52.

[18] Freitas, R., Henze, A., Meinke, M., Schröder, W. Analysis of Lattice-Boltzmann methods for internal flows. *Comput. Fluids* (2011) **47**(1):115–121.

[19] Eitel-Amor, G., Meinke, M., Schröder, W. A lattice-Boltzmann method with hierarchically refined meshes. *Comput. Fluids* (2013) **75**:127–139.

[20] Lintermann, A., Meinke, M., Schröder, W. Fluid mechanics based classification of the respiratory efficiency of several nasal cavities. *Comput. Biol. Med.* (2013) **43**(11):1833–1852.

[21] Lintermann, A., Schröder, W. A hierarchical numerical journey through the nasal cavity: from nose-like models to real anatomies. *Flow Turbul. Combust.* (2019) **102**(1):89–116.

[22] Bhatnagar, P. L., Gross, E. P., Krook, M. A model for collision processes in gases. i. small amplitude processes in charged and neutral one-component systems. *Phys. Rev.* (1954) **94**(3):511–525.

[23] Qian, Y. H., D'Humières, D., Lallemand, P. Lattice BGK Models for Navier-Stokes equation. *Europhysics Letters (EPL)* (1992) **17**(6):479–484.

[24] Benzi, R., Succi, S., Vergassola, M. The lattice Boltzmann equation: theory and applications. *Phys. Rep.* (1992) **222**(3):145–197.

[25] Lintermann, A., Schlimpert, S., Grimmen, J. H., Günther, C., Meinke, M., Schröder, W. Massively parallel grid generation on HPC systems. *Comput. Method Appl. M.* (2014) **277**:131–153.

[26] Fedorov A., Beichel R., Kalpathy-Cramer J., Finet J., Fillion-Robin J-C., Pujol S., Bauer C., Jennings D., Fennessy F., Sonka M., Buatti J., Aylward S.R., Miller J.V., Pieper S., Kikinis R. 3D Slicer as an image computing platform for the quantitative imaging network. *Magnetic Resonance Imaging* (2012) **30**(9):1323-41. PMID: 22770690.

[27] Ahmed, S. A., Giddens, D. P. Pulsatile poststenotic flow studies with Laser Doppler Anemometry. *J. Biomech.* (1984) **17**(9):695–705

[28] Gholampour, S. FSI simulation of CSF hydrodynamic changes in a large population of non-communicating hydrocephalus patients during treatment process with regard to their clinical symptoms. *PLoS ONE* (2018) **13**(4):e0196216.

[29] Krause, D. and Thörnig, P. JURECA: Modular supercomputer at Jülich Supercomputing Centre. *J. Large-Scale Research Facilities* (2018) **4**:A132.